RESEARCH ARTICLE
ATMOSPHERIC PHYSICS

*Earth and Planetary Physics*
*9*: 1–11, 2025
doi: 10.26464/epp2025006

# Impacts of ENSO on wintertime total column ozone over the Tibetan Plateau based on the historical simulations of community Earth system model

**XiaoWen Yuan, YuZhen Wang, Yang Li*, YuHao Liu, WeiLing Xu, LiZi Wang, and RuiHan Deng**

School of Atmospheric Sciences, Chengdu University of Information Technology, Chengdu 610225, China

**Key Points:**

- CESM2-WACCM and CESM2-WACCM-FV2 models can generally capture the climate mean and standard deviation of the wintertime TP TCO.
- El Niño (La Niña) corresponds to the TP TCO increase (decrease) by modifying the tropopause height in these two models, which is consistent with observations.
- These two models can basically capture the impact of ENSO on the TP TCO and its potential process.

**Citation:** Yuan, X. W., Wang, Y. Z., Li, Y., Liu, Y. H., Xu, W. L., Wang, L. Z., and Deng, R. H. (2025). Impacts of ENSO on wintertime total column ozone over the Tibetan Plateau based on the historical simulations of community Earth system model. *Earth Planet. Phys.*, *9*(2), 1–11. http://doi.org/10.26464/epp2025006

**Abstract:** The ozone over the Tibetan Plateau (TP) plays an important role in protecting the local ecology by absorbing ultraviolet solar rays. The El Niño-Southern Oscillation (ENSO), recognized as the strongest interannual climate phenomenon globally, can create ozone variations over the TP. Based on the historical experimental simulation results of two Community Earth System Models (i.e. CESM2-WACCM and CESM2-WACCM-FV2) that include the coupling process of stratospheric chemistry-radiation-dynamics, this study analyzes the impact of ENSO on the wintertime total ozone column (TCO) over the TP, as well as its physical processes, from 1979 to 2014. When compared to observations, the results show that the two models can basically simulate the spatial distribution of the climate state and standard deviation of the TP TCO. In the two models, CESM2-WACCM performs better. During the winter when the ENSO signal is strongest, its warm phase, El Niño, cools the tropospheric temperature over the TP by modifying the atmospheric circulation, which induces a decrease in the tropopause height. Such decreases in the tropopause height are responsible for the TP TCO increase. The cool phase La Niña is responsible for a TCO decrease over the TP, in a manner resembling the El Niño but with the opposite signal. Our results are consistent with previous observational analysis, and the relevant research provides valuable scientific insights for evaluating and improving the Earth System Model that incorporates the coupling process of stratospheric chemistry-radiation-dynamics.

**Keywords:** ENSO; Tibetan Plateau; total column ozone; wintertime; CESM2-WACCM; CESM2-WACCM-FV2

## 1. Introduction

The Tibetan Plateau (TP), the highest and largest plateau on Earth, is called the "Roof of the World" (Mo XX, 2010; Lu Q, 2021). Because of the special dynamic and thermal interactions of the TP, it has a profound influence on atmospheric circulation and climate variability (Mo XX, 2010; Kuang XX and Jiao JJ, 2016). There is the total column ozone (TCO) low centered over the TP, which has deepened over recent decades (Zhou XJ et al., 1995; Zou H et al., 2001; Bian JC et al., 2006; Liu Y et al., 2007; Li YC et al., 2023). Stratospheric ozone can effectively absorb harmful ultraviolet radiation ranging from 0.2 to 0.29 μm, preventing them from reaching the Earth's surface (Wang YQ et al., 2009; Chen XP et al., 2019). If the TCO over the TP diminishes, the amount of ultraviolet radiation received by the plateau surface will increase, harming the ecological environment and threatening human health (Zhu LGN and Wu ZW, 2023).

El Niño-Southern Oscillation (ENSO) is a phenomenon manifesting in the equatorial central and eastern Pacific Ocean, characterized by anomalous sea surface temperatures (SST) and quasi-periodic fluctuations. It is the most prominent interannual variability signal on Earth, with two distinct phases: the warm phase El Niño, and the cold phase La Niña (Miralles et al., 2014). To the linkage between ENSO and TP TCO, Zou H et al. (2001) and Chen P et al. (2023) have pointed out that El Niño events correspond to the TCO increase (positive anomalies) over the TP, and vice versa for La Niña events. Recently, Li Y et al. (2024) emphasized that the tropopause height change associated with ENSO contributes to the TCO anomalies over the TP. Specifically, the decrease (increase) of tropopause height during El Niño (La Niña) events

First author: X. W. Yuan, 3207369211@qq.com
Correspondence to: Y. Li, liyang0711@cuit.edu.cn
Received 22 AUG 2024; Accepted 15 NOV 2024.
First Published online 09 JAN 2025.

could carry ozone-rich (ozone-poor) stratospheric (tropospheric) air into the upper troposphere and lower stratosphere (UTLS) regions, inducing the positive (negative) TCO anomalies over the TP (Li Y et al., 2024).

Community Earth System Model version 2 — the Whole Atmosphere Community Climate Model (CESM2-WACCM) is a new generation of Earth system model developed by the National Center for Atmospheric Research (NCAR) in the United States (Gettelman et al., 2019). CESM2-WACCM considers the atmosphere, land, ocean, river, sea ice, land ice, as well as ocean waves, with WACCM6 representing its atmospheric component (Danabasoglu et al., 2020; Davis et al., 2023). In addition to the CESM2-WACCM model, there is another CESM2 as part of the Coupled Model Intercomparison Project Phase 6 (CMIP6), which is based on the CESM2-WACCM model and called CESM2-WACCM-FV2. Although the horizontal resolution of the atmosphere and land in the CESM2-WACCM-FV2 model has been reduced, the finite volume method is used in the dynamic core part, which may help to more accurately simulate the flow of the atmosphere and ocean (Eymard et al., 2000; Keeble et al., 2021). Previous studies have shown that the CESM-WACCM model can simulate the ozone dynamics over the TP and the impact of SST on ozone change well. For example, Zhang JK et al. (2015) demonstrated that WACCM3 has a good simulated performance of mid-latitude ozone change and its dynamic linkage with ENSO; Wan LF et al. (2017) successfully simulated the double-core structure of the summer ozone valley over the TP using WACCM3, and provided good simulation results for the center location of the UTLS ozone valley; Yu SY et al. (2022) utilized the historical simulations from WACCM to effectively reproduce the wave pattern of the climatological ozone; Li Y et al. (2024) used WACCM4 to analyze the impact of ENSO on summertime TCO low over the TP.

WACCM6 includes the coupling process of atmospheric chemistry-radiation-dynamics in the stratosphere. It is one of the best models in the CMIP6 for simulating the stratosphere and TCO (Gettelman et al., 2019; Keeble et al., 2021; Rao J et al., 2023a). Given the integration of the latest atmospheric chemistry-climate model (WACCM6) involved in the CESM2, we choose all CESM2 models available in CMIP6, which includes WACCM6: CESM2-WACCM and CESM2-WACCM-FV2. This study uses their historical simulation results to analyze the impact of ENSO on TCO over the TP and its potential physical processes during winter (December–January–February; DJF), when the interannual variation of TP TCO (Figure S1) and ENSO (Timmermann et al., 2018; Li Y et al., 2024) are strongest.

This study focuses the following key questions: (1) What is the performance of the CESM2-WACCM and CESM2-WACCM-FV2 models in simulating the climate mean and variability of wintertime TP TCO? (2) Can these two models capture the statistical correlation and physical linkage between wintertime ENSO and TP TCO? These studies could not only help to deepen our understanding of the mechanisms underlying the interannual variation of TP TCO, but also demonstrate the capabilities of the new generation of CESM models in reproducing ozone changes over the TP.

## 2. Data and Methods

### 2.1 Data

The TCO observational data utilized in this study originated from merged satellite records provided by the Copernicus Climate Change Service (C3S), with a horizontal resolution of 0.5° × 0.5°. The satellite data merged 15 satellite sensors, including the Global Ozone Monitoring Experiment (GOME, 1995–2011), Scanning Imaging Absorption Spectrometer for Atmospheric Chartography (SCIAMACHY, 2002–2012), Ozone Monitoring Instrument (OMI, 2004–present), GOME-2A/B (2007–present), Backscatter Ultraviolet Radiometer (BUV-Nimbus4, 1970–1980), Total Ozone Mapping Spectrometer (TOMS-EP, 1996–2006), a series of Solar Backscatter Ultraviolet Radiometers (SBUV, 1985–present), and Ozone Mapping and Profiler Suite (OMPS, 2012–present). This dataset's monthly gridded average TCO values exhibit long-term stability of less than 1% per decade. The systematic and random errors of the data are below 2% and 3–4%, respectively (Li YJ et al., 2020; Li Y et al., 2024). The historical simulations of CESM2-WACCM and CESM2-WACCM-FV2 models include mole fraction of ozone, air pressures, temperatures, geopotential heights, and sea surface temperatures. CESM2-WACCM model has a horizontal resolution of 0.9° × 1.25°, while the CESM2-WACCM-FV2 model has a resolution of 1.9° × 2.5° (Keeble et al., 2021; Mmame et al., 2023). The simulations for both models are provided by CMIP6, covering the pressure levels from 1000 hPa to 1 hPa. Given that the satellite observation data began in 1979 and the model's historical simulations ended in 2014, we select the overlapping period of all data in this study (1979–2014). The anomalies represent the deseasonalised anomalies with respect to the period 1979–2014. The monthly sea surface temperature (SST) data is provided by the Hadley Centre Sea Ice and SST dataset version 1 (HadISST1), which has a resolution of 1.0° × 2.5° (Rayner et al., 2003). Following previous studies (e.g. Li Y et al., 2024), we selected the latitude–longitude domain of 27.5–37.5°N, 75.5–105.5°E as the TP region. Furthermore, the boundary of the TP region is based on the study by Zhang YL et al. (2002). In addition, the Niño 3.4 index from the National Oceanic and Atmospheric Administration's (NOAA) Climate Prediction Center (CPC) is used in this study to represent ENSO.

### 2.2 Methods

For the tropopause height, this study follows the thermodynamic definition put forth by the World Meteorological Organization (WMO). The tropopause height is defined as the lowest level at which the lapse rate decreases to 2 K/km or less, provided that the average lapse rate between this level and all higher levels within 2 km does not exceed 2 K/km (WMO, 1957). Based on the relationship between altitude and air pressure, the average temperature $\bar{T}$ between the two isobaric surfaces $P_1$ and $P_2$ is (Wallace et al., 1998; Holton and Hakim, 2013; Sun C et al., 2017):

$$\bar{T} = \frac{g}{R} \times \left( \ln \frac{P_1}{P_2} \right)^{-1} \times \Delta Z,$$

where $g$ and $R$ represent 9.80665 m·s$^{-2}$ and 287 J·kg$^{-1}$·K$^{-1}$, respectively. $\Delta Z$ represents the difference in geopotential height between the two isobaric surfaces. If $\Delta Z$ in Equation (1) is the time-averaged perturbation value $\Delta Z'$, then the perturbation value of

the average temperature $\Delta T'$ is:

$$\Delta T' = \frac{g}{R} \times \left( \ln \frac{P_1}{P_2} \right)^{-1} \times \Delta Z'.$$

From Equation (2), the perturbation of the average temperature between the two isobaric layers $P_1$ and $P_2$ is proportional to the thickness of the perturbation. Specifically, if the perturbed layer becomes thinner (thicker), the mean temperature within that layer should decrease (increase). Consequently, Equation (2) is used in this study to discuss the effect of atmospheric thickness on tropospheric temperature (Wallace et al., 1998; Sun C et al., 2017; Zhang YZ et al., 2022).

Pearson correlation coefficient is used to investigate the statistical relationship between ENSO and TP TCO. This study utilizes the two-tailed Student's t-test to examine the significance of the correlation coefficient (Pearson, 1894; Lomax and Hahs-Vaughn, 2013).

## 3. Results

### 3.1 Assessment of CESM2-WACCM, CESM2-WACCM-FV2 Models

Figure 1 shows the spatial pattern of the wintertime TCO climate mean and its standard deviation over the TP in the C3S satellite observations and simulations of CESM2-WACCM and CESM2-WACCM-FV2 models. Comparing the three spatial patterns in Figures 1a–1c, it is suggested that the TCO climate mean from the two models is basically consistent with that of observations. Furthermore, all of them show significant latitudinal characteristics, with a decreasing of TCO value from the northern to the southern part of the TP. Figures 1d–1f show the standard deviation of TP TCO during winter for both the satellite observations and the two models. In addition to the climate mean, these two models can capture the latitudinal characteristics of standard deviation in observations (Figures 1d–1f). It can be seen from Figure 1f that the standard deviation of CESM2-WACCM-FV2 is larger relative to the observations, and also larger than that of CESM2-WACCM (Figures 1d–1e). It is indicated that the CESM2-WACCM-FV2 model has a larger wintertime interannual variability, which may be due to its higher horizontal resolution. Comparing the standard deviation in Figures 1d–1f, the simulation of the CESM2-WACCM model seems to be closer to observations, suggesting that CESM2-WACCM has a better simulation performance in wintertime interannual variability of TP TCO. Furthermore, the spatial correlation coefficients for the TP TCO between the models and observations are all greater than 0.9, while those for the standard deviation exceed 0.8. In particular, the CESM2-WACCM model exhibits higher spatial correlation compared to CESM2-WACCM-FV2. Overall, these two models can basically reproduce the latitudinal characteristics of wintertime climate mean and standard deviation in the TP TCO, despite some biases in the models. In particular, the CESM2-WACCM model better captures the wintertime standard deviation of TP TCO.

### 3.2 Statistical Relationship Between ENSO and TCO over the TP

Figure 2 shows the positive correlation between TCO anomalies over the TP and ENSO during winter in the CESM2-WACCM and CESM2-WACCM-FV2 models. Specifically, for El Niño (La Niña), a significant increase (decrease) in SST in the equatorial east-central Pacific Ocean corresponds to significant positive (negative) TCO anomalies over the TP. These results from models (Figure 2) are consistent with those of previous studies by Zou H et al. (2001) and Li Y et al. (2024). To further validate the relationship, the correlation of spatial pattern between the wintertime SST anomalies in the tropical Pacific (30°N–30°S, 120°E–80°W) (Rasmusson

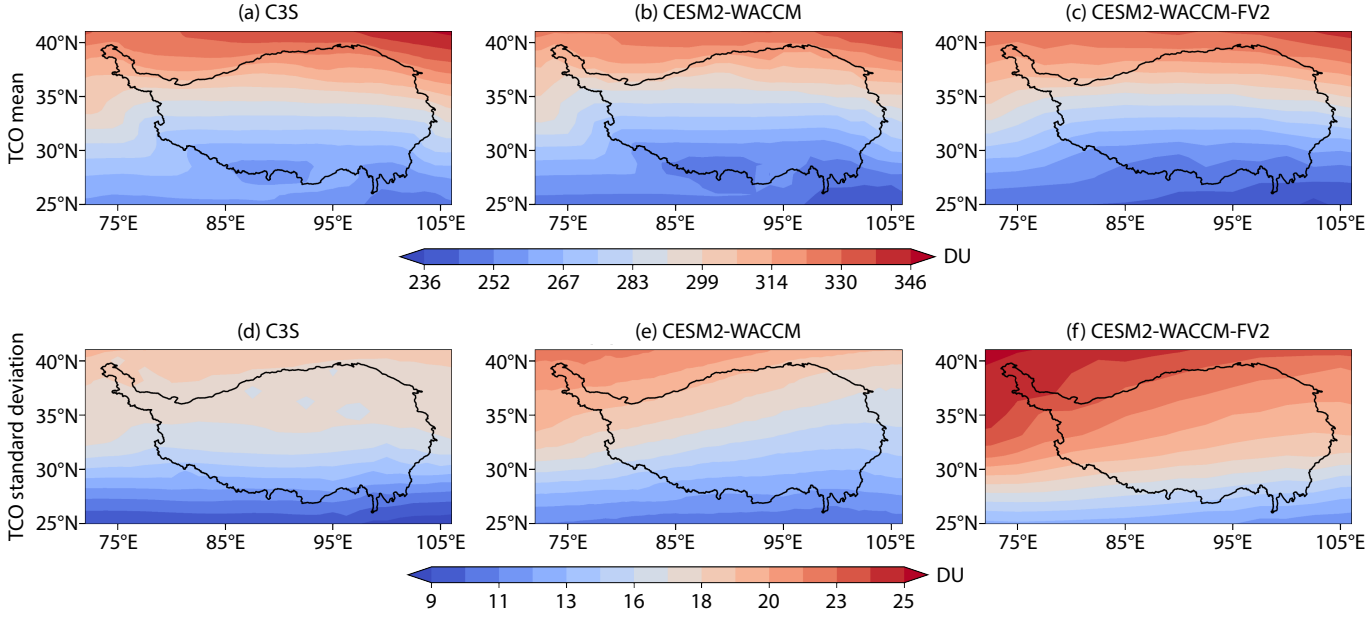


**Figure 1**. (a–c) Climate mean state and (d–f) standard deviation of total column ozone (TCO, Unit: DU) over the Tibetan Plateau (TP) during winter (December–January–February; DJF), from 1979 to 2014, for C3S satellite observation, CESM2-WACCM model, and CESM2-WACCM-FV2 model.

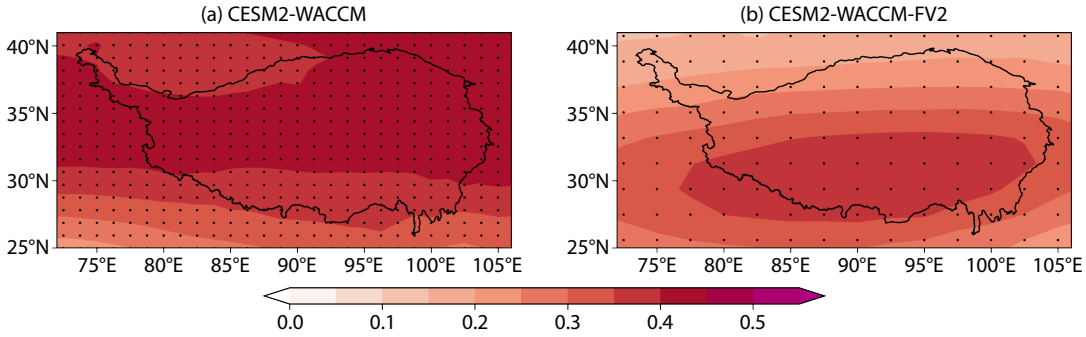


**Figure 2**. The correlation pattern between the TCO anomalies over the TP and the Niño3.4 index during winter from 1979 to 2014 for the (a) CESM2-WACCM and (b) CESM2-WACCM-FV2 model simulations. Dotted regions indicate statistical significance at the 90% confidence level.

and Carpenter, 1982; Li Y et al., 2019) and the time series of anomalous TP TCO is plotted (Figure 3). Figure 3a shows the correlation between SST anomalies and TP TCO anomalies, and we find that there is a strong positive correlation in the eastern tropical Pacific. Compared with Figures 3a–3c, it is found that the simulations are roughly consistent with observations. Particularly, the CESM2-WACCM model seems to perform a better simulation, because the significantly positive correlation of CESM2-WACCM-FV2 extends to the western tropical Pacific. As shown in Figures 3b–3c, these two models have a significant positive correlation between the tropical Pacific SST anomalies and TCO anomalies over the TP during winter. In addition, the significant spatial distribution shows a "seesaw" pattern of warming and cooling between the eastern and western tropical Pacific (Figure 3), which is similar to the spatial pattern of ENSO. When the TCO anomalies over the TP increase (decrease), it corresponds to the warming (cooling) of the tropical east-central Pacific (Figure 3). This indicates that the linkage between the TCO anomalies over the TP and the ENSO is consistent with that of observations (Li Y et al., 2024).

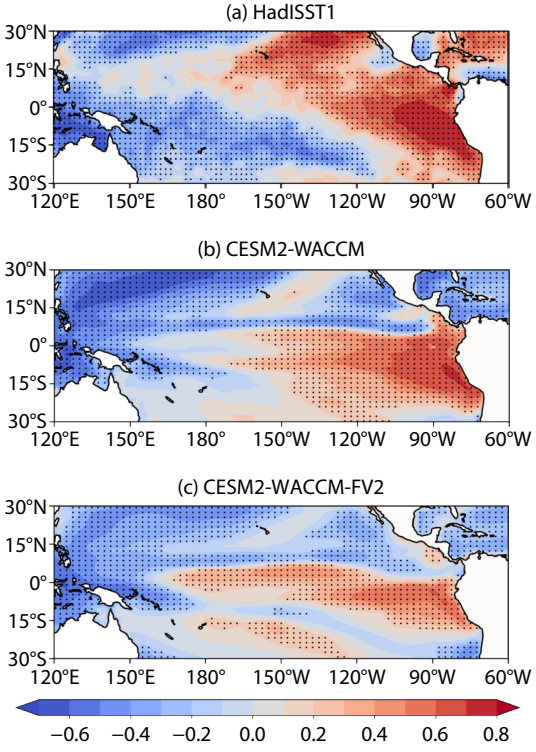


**Figure 3**. The correlation pattern between the sea surface temperature (SST) anomalies and the time series of TP TCO anomalies during winter from 1979 to 2014, for (a) observations, and the (b) CESM2-WACCM and (c) CESM2-WACCM-FV2 model simulations. Dotted regions indicate statistical significance at the 90% confidence level.

### 3.3 Physical Linkage Between ENSO and TCO over the TP

The TCO is the sum of the partial column ozone (PCO) from the surface to the top of the atmosphere (Ziemke et al., 2001). To better understand the influence of ENSO on the TP TCO, Figure 4 shows the correlation coefficients between PCO over the TP and ENSO at different pressure levels for the CESM2-WACCM and CESM2-WACCM-FV2 simulations. With the increasing altitude, the correlation coefficients between PCO and ENSO exhibit an upward trend until 50 hPa. It is noted that their correlation peaks at 150 hPa, at an altitude is consistent with the wintertime mean tropopause height over the TP (Li Y et al., 2024). In addition, the correlation between PCO and ENSO is significant within the pres-

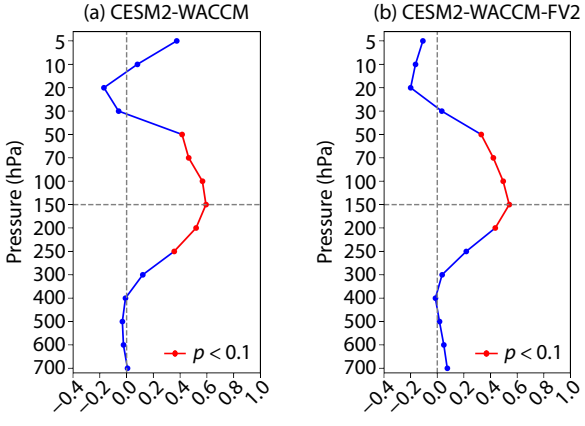


**Figure 4**. The correlation between partial column ozone (PCO) anomalies over the TP and the Niño3.4 index during winter from 1979 to 2014 for the (a) CESM2-WACCM and (b) CESM2-WACCM-FV2 model simulations. The horizontal gray dashed line represents 150 hPa pressure layer, the vertical gray dashed line represents the correlation coefficient zero line, and the red curve represents the correlations that exceed the 90% confidence level or the probability value that is less than 0.1 ($p < 0.1$).

sure range from 250 to 50 hPa in CESM2-WACCM model ($p < 0.1$, red area in Figure 4a). Similarly, it is significant within the pressure range from 200 to 50 hPa in CESM2-WACCM-FV2 model (Figure 4b). The pressure layers that pass the significance test are essentially the same for both models, concentrated in the UTLS region of TP. In addition, we investigated the vertical profile of the correlation between the percentage change in ozone concentration over the TP and ENSO (Figure S2), which is consistent with that of PCO (Figure 4). In the CESM2-WACCM and CESM2-WACCM-FV2 models, these results indicate that ENSO could affect the PCO change in the UTLS region and thus contribute to the TCO anomalies over the TP. This is consistent with analysis of the observations (Li Y et al., 2024), and further demonstrates the ability of these two models to simulate the influence of ENSO on the TP TCO.

The tropopause serves as the boundary between the stratosphere and the troposphere. Many studies have found that there is a strong correlation between the tropopause height and TCO (Zhang JK et al., 2015; Li Y et al., 2024). Atmospheric ozone is mainly concentrated in the stratosphere and less in the troposphere. When the tropopause rises (descends), the atmosphere of the troposphere will become thicker (thinner) and the atmosphere of the stratosphere will become thinner (thicker), corresponding to a decrease (increase) in TCO (Tung and Yang H, 1988; Steinbrecht et al., 1998; Li GH et al., 2003). Based on the results in Figure 4, this study finds that the significant correlation between ENSO and PCO occurs in the UTLS region, with the strongest correlation observed at 150 hPa. Given that the wintertime average tropopause height over the TP is about 150 hPa, this further suggests the potential influence of tropopause height variations on the TP TCO. Figure 5 shows the correlation between ENSO and tropopause pressure over the TP during winter. This result indicates that the two models exhibit a significant positive correlation between ENSO and tropopause pressure, with the significant anomaly roughly located between 30°–35°N (Figure 5). The positive correlation suggests that the El Niño (La Niña) events correspond to the increasing (decreasing) tropopause pressure over the TP, which is consistent with the results of the observational analysis (Li Y et al., 2024).

Based on the results in Figures 2–5, it is known that the TCO anomalies associated with ENSO are linked to the tropopause height change over the TP. It has been pointed out that troposphere air temperature could induce changes in tropopause height (Seidel and Randel, 2006; Peethani et al., 2014). ENSO can affect the tropopause height via modulating the tropospheric temperature over the TP (Li Y et al., 2024). How, then, does ENSO induce the change of tropospheric air temperature over the TP? According to Equation (2), the upper-level atmospheric circulation can change the tropospheric air temperature by modifying atmospheric thickness. Specifically, an increase (decrease) in the geopotential height of the upper troposphere leads to warming (cooling) of the tropospheric air temperature (Wallace et al., 1998; Sun C et al., 2017; Zhang YZ et al., 2022).

Since the wintertime climate mean of tropopause height over the the whole TP region is roughly located at 150 hPa, we will investigate the correlation between the 150 hPa geopotential height anomalies and ENSO in the two models (Figures 6a–6b). There is a significant negative correlation in the two models, indicating that the El Niño events corresponds to negative geopotential height anomalies over the TP, and vice versa for the La Niña. The anomalous geopotential height of 150 hPa associated with ENSO could be attributed partly to atmospheric teleconnections from the tropical Pacific and Indian Oceans, and partly to the thermal dynamics between the Indian Ocean and the plateau. (Li Y et al., 2024). Based on equation (2), if upper level geopotential height cause the increasing air thickness, the tropospheric air temperature associated with thickness (Tthickness) will warm. In this study, the Tthickness over the TP at 700–150 hPa for the CESM2-WACCM and CESM2-WACCM-FV2 models is calculated by using equation (2). As shown in Figures 6c–6d, there is a significantly negative correlation between Tthickness and ENSO. In the simulations provided by the two models, it is noted that these negative correlations are stronger in the southern region of the TP (Figures 6c–6d). These patterns are consistent with the distribution of the correlation results of the tropopause heights. This indicates that 150 hPa geopotential height anomalies play a key role in the Tthickness, which is modulated by the upper atmospheric circulation.

From the above analysis, it is evident that the CESM2-WACCM and CESM2-WACCM-FV2 models could reproduce the physical linkage between ENSO and TP TCO. In cases where the geopotential height of 150 hPa associated with El Niño (La Niña) decreases (increases), the atmospheric thickness decreases (increases) and

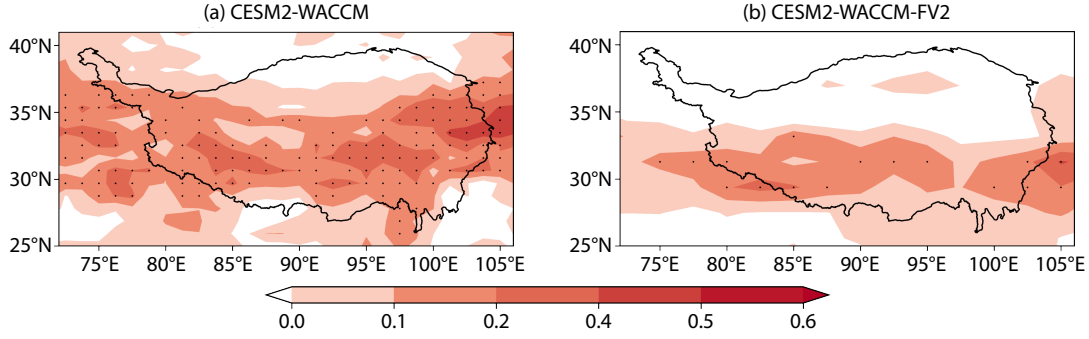


**Figure 5**. The correlation pattern between the tropopause pressure anomalies over the TP and the Niño3.4 index during winter from 1979 to 2014, for the (a) CESM2-WACCM and (b) CESM2-WACCM-FV2 model simulations. Dotted regions indicate statistical significance at the 90% confidence level.

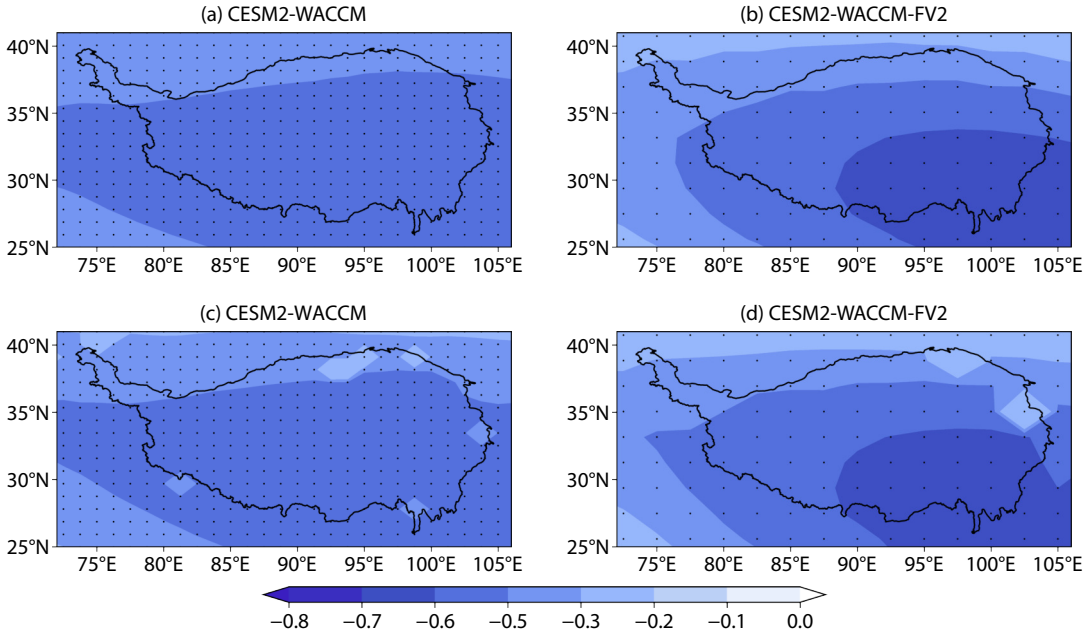


**Figure 6**. The correlation pattern between the wintertime Niño3.4 index and (a–b) 150 hPa geopotential height anomalies over the TP, as well as (c–d) the air temperature associated with the thickness of the TP from 1979 to 2014 for the CESM2-WACCM and CESM2-WACCM-FV2 model simulations. Dotted regions indicate statistical significance at the 90 % confidence level.

thus cools (warms) the tropospheric temperature, which in turn induces a lowering (raising) of the tropopause height. Such tropopause height decrease (increase) is responsible for the increase (decrease) in the TP TCO. This is consistent with the results of Li Y et al. (2024), which are based on observations, indicating that the CESM2-WACCM and CESM2-WACCM-FV2 models could effectively capture the influence of ENSO on TCO over the TP and its associated potential process.

## 4. Conclusion and Discussion

Based on the latest generation of Earth system models CESM2-WACCM and CESM2-WACCM-FV2, which incorporate the coupling process of stratospheric chemistry-radiation-dynamics, this study evaluated their simulation capabilities in modeling the impact of ENSO on TCO over the TP. Our conclusions are as follows:

(1) The CESM2-WACCM and CESM2-WACCM-FV2 models can basically simulate the latitudinal characteristics of wintertime climate mean and standard deviation in the TP TCO, despite some biases in the models. Both models exhibit a decreasing zonal pattern from north to south. Particularly, CESM2-WACCM performs better in capturing the wintertime standard deviation of TP TCO, which may be due to its higher resolution than CESM2-WACCM-FV2 (Rao J et al., 2023a, b). Additionally, the CESM2-WACCM model better reproduces the QBO signal than CESM2-WACCM-FV2, which may be responsible for the TCO variability through the influence of the QBO on TCO (Randel et al., 2011; Zhang JK et al., 2021; Wang WK et al., 2022; Rao J et al., 2023a, b). In addition, ENSO is a global-scale interannual variability, affecting not only TP TCO but also TCO in the East Asian and Pacific regions (Figures S3–S7).

(2) In the CESM2-WACCM and CESM2-WACCM-FV2 models, there is significant positive correlation between the TCO anomalies over the TP and ENSO during winter. Specifically, El Niño (La Niña) corresponds to significant positive (negative) TCO anomalies over the TP. In addition, compared with other areas at the same latitude, the ozone over the TP is significantly lower, indicating the presence of an ozone low center over the TP (Rao J and Garfinkel, 2020; Li Y et al., 2024). We found that there is a positive correlation between the zonal TCO anomalies over the TP and ENSO in both models (Figure S8). The larger the zonal TCO anomalies, the weaker the ozone low center, which suggests that El Niño (La Niña) weakens (strengthens) the ozone low center (Figure S8).

(3) The significant correlation between ENSO and PCO occurs in the UTLS region, with the strongest correlation observed at 150 hPa, which is the wintertime average of tropopause height over the TP. Both models exhibit a significant positive correlation between ENSO and tropopause height, suggesting that the El Niño (La Niña) events correspond to the increasing (decreasing) tropopause height over the TP.

(4) Based on the historical experimental simulation results of two Community Earth System Models, CESM2-WACCM and CESM2-WACCM-FV2, the main physical mechanism behind the positive correlation between ozone over the TP and ENSO is as follows: If an El Niño (La Niña) event occurs, the geopotential height of 150 hPa decreases (increases), and the atmospheric thickness decreases (increases), thereby causing the cooling (warming) tropospheric temperature, which in turn induces a decreasing (increasing) of the tropopause height. The decrease (increase) in tropopause height leads to the increasing (decreasing) TCO over the TP. The results of the two models are basically consistent with observations (Li Y et al., 2024), indicating that these two models can basically capture the impact of ENSO on the TCO over the TP and its potential process. In addition, Shen L et al. (2024) explored the possible reasons for the positive correlation between ozone over the TP and ENSO from stationary transport. They pointed out

that the stationary transport has a larger impact on the ozone valley formation than the transient transport (Shen L et al., 2024). The eddy-driven stationary ozone transport flux significantly impacts the development of low ozone centers over the TP, which shows the significance of such eddies in the formation of the ozone valleys over high-terrain regions (Shen L et al., 2024). This further indicates that the physical mechanism of the linkage between ENSO and TP TCO may be also related to the influence of eddy-driven ozone transport (Shen L et al., 2024). Considering that we focus on the potential impact of tropopause change associated with ENSO on TP TCO, future work is needed for a better understanding of TP TCO change, through investigating the synergistic impact of eddy-driven ozone transport and tropopause change.

## Acknowledgements

This work was jointly supported by the National Natural Science Foundation of China (grant Nos. U2442210, 42175042, 42275059), the Natural Science Foundation of Sichuan Province (grant Nos. 2024NSFTD0017, 2023NSFSC0246), and the Second Tibetan Plateau Scientific Expedition and Research (STEP) program (2019QZKK0103). We acknowledge the Copernicus Climate Change Service for supporting the C3S satellite product (https://doi.org/10.24381/cds.4ebfe4eb), and the Coupled Model Intercomparison Project Phase 6 (CMIP6) for supporting the CESM2-WACCM and CESM2-WACCM-FV2 model data (https://pcmdi.llnl.gov/CMIP6/).

## References

Bian, J. C., Wang, G. C., Chen, H. B., Qi, D. L., Lü, D. R., and Zhou, X. J. (2006). Ozone mini-hole occurring over the Tibetan Plateau in December 2003. *Chin. Sci. Bull.*, *51*(7), 885–888. https://doi.org/10.1007/s11434-006-0885-y

Chen, P., Li, Y. C., Jing, G. L., and Chang, S. J. (2023). Analysis of the Qinghai-Xizang Plateau ozone valley of stratospheric formation mechanism. *Plateau Meteor. (in Chinese)*, *42*(5), 1182–1193. https://doi.org/10.7522/j.issn.1000-0534.2022.00106

Chen, X. P., Xian, L., Ju, T. Z., Zhang, J. Y., Wang, P. Y., Liu, H. Q., and Pei, J. (2019). Study of spatial and temporal distribution of ozone and its influencing factors in Ningxia based on OMI. *J. Ecol. Rural Environ. (in Chinese)*, *35*(2), 167–173. https://doi.org/10.19741/j.issn.1673-4831.2017.0831

Danabasoglu, G., Lamarque, J. F., Bacmeister, J., Bailey, D. A., DuVivier, A. K., Edwards, J., Emmons, L. K., Fasullo, J., Garcia, R., … Strand, W. G. (2020). The community earth system model version 2 (CESM2). *J. Adv. Model. Earth Syst.*, *12*(2), e2019MS001916. https://doi.org/10.1029/2019MS001916

Davis, N. A., Visioni, D., Garcia, R. R., Kinnison, D. E., Marsh, D. R., Mills, M., Richter, J. H., Tilmes, S., Bardeen, C. G., … Vitt, F. (2023). Climate, variability, and climate sensitivity of "Middle atmosphere" chemistry configurations of the community Earth system model version 2, whole atmosphere community climate model version 6 (CESM2 (WACCM6)). *J. Adv. Model. Earth Syst.*, *15*(9), e2022MS003579. https://doi.org/10.1029/2022MS003579

Eymard, R., Gallouët, T., and Herbin, R. (2000). Finite volume methods. In P. G. Ciarlet, et al. (Eds.), *Handbook of Numerical Analysis* (vol. 7, pp. 713–1018). Amsterdam: Elsevier. https://doi.org/10.1016/S1570-8659(00)07005-8

Gettelman, A., Mills, M. J., Kinnison, D. E., Garcia, R. R., Smith, A. K., Marsh, D. R., Tilmes, S., Vitt, F., Bardeen, C. G., … Randel, W. J. (2019). The whole atmosphere community climate model version 6 (WACCM6). *J. Geophys. Res.: Atmos.*, *124*(23), 12380–12403. https://doi.org/10.1029/2019JD030943

Holton, J. R., and Hakim, G. J. (2013). *An Introduction to Dynamic Meteorology* (5th ed). Burlington: Academic Press. https://doi.org/10.1016/C2009-0-63394-8

Keeble, J., Hassler, B., Banerjee, A., Checa-Garcia, R., Chiodo, G., Davis, S., Eyring, V., Griffiths, P. T., Morgenstern, O., … Wu, T. (2021). Evaluating stratospheric ozone and water vapour changes in CMIP6 models from 1850 to 2100. *Atmos. Chem. Phys.*, *21*(6), 5015–5061. https://doi.org/10.5194/acp-21-5015-2021

Kuang, X. X., and Jiao, J. J. (2016). Review on climate change on the Tibetan Plateau during the last half century. *J. Geophys. Res.: Atmos.*, *121*(8), 3979–4007. https://doi.org/10.1002/2015JD024728

Li, G. H., Lü, D. R., and Tie, X. X. (2003). The impact of tropopause variation on ozone distribution in upper troposphere/lower stratosphere. *Chin. J. Space Sci. (in Chinese)*, *23*(4), 269–277. https://doi.org/10.3969/j.issn.0254-6124.2003.04.005

Li, Y., Chen, Q. L., Cai, H. K., and Wang, Z. L. (2019). Long term trend of tropical Pacific temperature under global warming. *Climatic Environ. Res. (in Chinese)*, *24*(6), 723–734. https://doi.org/10.3878/j.issn.1006-9585.2018.18072

Li, Y., Feng, W. H., Zhou, X., Li, Y. J., and Chipperfield, M. P. (2024). The impact of El Niño–Southern Oscillation on the total column ozone over the Tibetan Plateau. *Atmos. Chem. Phys.*, *24*(14), 8277–8293. https://doi.org/10.5194/acp-24-8277-2024

Li, Y. C., Xu, F., Wan, L. F., Chen, P., Guo, D., Chang, S. J., and Yang, C. (2023). Effect of ENSO on the ozone valley over the Tibetan Plateau based on the WACCM4 model. *Remote Sens.*, *15*(2), 525. https://doi.org/10.3390/rs15020525

Li, Y. J., Chipperfield, M. P., Feng, W. H., Dhomse, S. S., Pope, R. J., Li, F. Q., and Guo, D. (2020). Analysis and attribution of total column ozone changes over the Tibetan Plateau during 1979–2017. *Atmos. Chem. Phys.*, *20*(14), 8627–8639. https://doi.org/10.5194/acp-20-8627-2020

Liu, Y., Guo, C. L., Li, W. L., and Zhou, X. J. (2007). Trends of stratospheric ozone and aerosols over Tibetan Plateau. *Acta Meteor. Sin. (in Chinese)*, *65*(6), 938–945. https://doi.org/10.3321/j.issn:0577-6619.2007.06.011

Lomax, R. G., and Hahs-Vaughn, D. L. (2013). *Statistical Concepts-A Second Course* (4th ed). New York: Routledge. https://doi.org/10.4324/9780203137802

Lu, Q. (2021). Characteristics of ozone low value center over Qinghai Tibet Plateau in summer. *Agric. Technol. Equip. (in Chinese)*, (7), 142–143,145. https://doi.org/10.3969/j.issn.1673-887X.2021.07.065

Miralles, D. G., Van Den Berg, M. J., Gash, J. H., Parinussa, R. M., de Jeu, R. A. M., Beck, H. E., Holmes, T. R. H., Jiménez, C., Verhoest, N. E. C., … Dolman, A. J. (2014). El Niño–La Niña cycle and recent trends in continental evaporation. *Nat. Clim. Chang.*, *4*(2), 122–126. https://doi.org/10.1038/nclimate2068

Mmame, B., Sunitha, P., Samatha, K., Rao, S. R., Satish, P., Amasarao, A., and Sekhar, K. C. (2023). Assessment of CMIP6 model performance in simulating atmospheric aerosol and precipitation over Africa. *Adv. Space Res.*, *72*(8), 3096–3108. https://doi.org/10.1016/j.asr.2023.06.030

Mo, X. X. (2010). A review and prospect of geological researches on the Qinghai-Tibet Plateau. *Geol. China (in Chinese)*, *37*(4), 841–853. https://doi.org/10.3969/j.issn.1000-3657.2010.04.002

Pearson, K. (1894). III. Contributions to the mathematical theory of evolution. *Phil. Trans. Roy. Soc. Lond. A*, *185*, 71–110. https://doi.org/10.1098/rsta.1894.0003

Peethani, S., Sharma, N., and Pathakoti, M. (2014). Effect of tropospheric and stratospheric temperatures on tropopause height. *Remote Sens. Lett.*, *5*(11), 933–940. https://doi.org/10.1080/2150704X.2014.973078

Randel, W. J., and Thompson, A. M. (2011). Interannual variability and trends in tropical ozone derived from SAGE II satellite data and SHADOZ ozonesondes. *J. Geophys. Res.: Atmos.*, *116*(D7), D07303. https://doi.org/10.1029/2010JD015195

Rao, J., and Garfinkel, C. I. (2020). Arctic ozone loss in March 2020 and its seasonal prediction in CFSv2: A comparative study with the 1997 and 2011 cases. *J. Geophys. Res.: Atmos.*, *125*(21), e2020JD033524. https://doi.org/10.1029/2020JD033524

Rao, J., Garfinkel, C. I., Ren, R. C., Wu, T. W., and Lu, Y. X. (2023a). Southern hemisphere response to the quasi-biennial oscillation in the CMIP5/6 models. *J. Climate*, *36*(8), 2603–2623. https://doi.org/10.1175/JCLI-D-22-0675.1

Rao, J., Garfinkel, C. I., Ren, R. C., Wu, T. W., Lu, Y. X., and Chu, M. (2023b). Projected strengthening impact of the Quasi-Biennial Oscillation on the

Southern Hemisphere by CMIP5/6 models. *J. Climate*, *36*(16), 5461–5476. https://doi.org/10.1175/JCLI-D-22-0801.1

Rasmusson, E. M., and Carpenter, T. H. (1982). Variations in tropical sea surface temperature and surface wind fields associated with the Southern Oscillation/El Niño. *Mon. Wea. Rev.*, *110*(5), 354–384. https://doi.org/10.1175/1520-0493(1982)110<0354:VITSST>2.0.CO;2

Rayner, N. A. A., Parker, D. E., Horton, E. B., Folland, C. K., Alexander, L. V., Rowell, D. P., ... and Kaplan, A. (2003). Global analyses of sea surface temperature, sea ice, and night marine air temperature since the late nineteenth century. *J. Geophys. Res.: Atmos.*, 108(D14). https://doi.org/10.1029/2002JD002670

Seidel, D. J., and Randel, W. J. (2006). Variability and trends in the global tropopause estimated from radiosonde data. *J. Geophys. Res.: Atmos.*, *111*(D21), D21101. https://doi.org/10.1029/2006JD007363

Shen, L., Rao, J., Guo, D., Yang, J. F., and Wang, Q. L. (2024). Comparison of the climatic characteristics of ozone valley over the Tibetan Plateau and the Rocky Mountains. *Earth Space Sci.*, *11*(4), e2023EA003379. https://doi.org/10.1029/2023EA003379

Steinbrecht, W., Claude, H., Köhler, U., and Hoinka, K. P. (1998). Correlations between tropopause height and total ozone: Implications for long-term changes. *J. Geophys. Res.: Atmos.*, *103*(D15), 19183–19192. https://doi.org/10.1029/98JD01929

Sun, C., Li, J. P., Ding, R. Q., and Jin, Z. (2017). Cold season Africa–Asia multidecadal teleconnection pattern and its relation to the Atlantic multidecadal variability. *Climate Dyn.*, *48*(11), 3903–3918. https://doi.org/10.1007/s00382-016-3309-y

Timmermann, A., An, S. I., Kug, J. S., Jin, F. F., Cai, W. J., Capotondi, A., Cobb, K. M., Lengaigne, M., McPhaden, M. J., … Zhang, X. B. (2018). El Niño–southern oscillation complexity. *Nature*, *559*(7715), 535–545. https://doi.org/10.1038/s41586-018-0252-6

Tung, K. K., and Yang, H. (1988). Dynamic variability of column ozone. *J. Geophys. Res.: Atmos.*, *93*(D9), 11123–11128. https://doi.org/10.1029/JD093iD09p11123

Wallace, J. M., Rasmusson, E. M., Mitchell, T. P., Kousky, V. E., Sarachik, E. S., and von Storch, H. (1998). On the structure and evolution of ENSO-related climate variability in the tropical Pacific: Lessons from TOGA. *J. Geophys. Res.: Oceans*, *103*(C7), 14241–14259. https://doi.org/10.1029/97JC02905

Wan, L. F., Guo, D., Liu, R. Q., Shi, C. H., and Su, Y. C. (2017). Evaluation of WACCM3 performance on simulation of the double core of ozone valley over the Qinghai-Xizang in summer. *Plateau Meteor. (in Chinese)*, *36*(1), 57–66. https://doi.org/10.7522/j.issn.1000-0534.2016.00004

Wang, W. K., Hong, J., Shangguan, M., Wang, H. Y., Jiang, W., and Zhao, S. Y. (2022). Zonally asymmetric influences of the quasi-biennial oscillation on stratospheric ozone. *Atmos. Chem. Phys.*, *22*(20), 13695–13711. https://doi.org/10.5194/acp-22-13695-2022

Wang, Y. Q., Jiang, H., Xiao, Z. Y., Zhang, X. Y., Zhou, G. M., and Yu, S. Q. (2009). Extracting temporal and spatial distribution information about total ozone amount in China based on OMI satellite data. *Environ. Sci. Technol. (in Chinese)*, *32*(6), 177–180,184. https://doi.org/10.3969/j.issn.1003-6504.2009.06.041

World Meteorological Organization. (1957). Meteorology—A three-dimensional science: Second session of the commission for aerology. *WMO Bull.*, *4*(4), 134–138.

Yu, S. Y., Rao, J., and Guo, D. (2022). Arctic ozone loss in early spring and its impact on the stratosphere-troposphere coupling. *Earth Planet. Phys.*, *6*(2), 177–190. https://doi.org/10.26464/epp2022015

Zhang, J. K., Tian, W. S., Wang, Z. W., Xie, F., and Wang, F. Y. (2015). The influence of ENSO on northern midlatitude ozone during the winter to spring transition. *J. Climate*, *28*(12), 4774–4793. https://doi.org/10.1175/JCLI-D-14-00615.1

Zhang, J. K., Zhang, C. Y., Zhang, K. Q., Xu, M., Duan, J. K., Chipperfield, M. P., Feng, W. H., Zhao, S. Y., and Xie, F. (2021). The role of chemical processes in the quasi-biennial oscillation (QBO) signal in stratospheric ozone. *Atmos. Environ.*, *244*, 117906. https://doi.org/10.1016/j.atmosenv.2020.117906

Zhang, Y. L., Li, B. Y., and Zheng, D. (2002). A discussion on the boundary and area of the Tibetan Plateau in China. *Geogr. Res. (in Chinese)*, *21*(1), 1–8. https://doi.org/10.11821/yj2002010001

Zhang, Y. Z., Li, J. P., Hou, Z. L., Zuo, B., Xu, Y. D., Tang, X. X., and Wang, H. (2022). Climatic effects of the Indian Ocean tripole on the Western United States in boreal summer. *J. Climate*, *35*(8), 2503–2523. https://doi.org/10.1175/JCLI-D-21-0490.1

Zhou, X. J., Luo, C., Li, W. L., and Shi, J. E. (1995). Ozone changes over China and low center over Tibetan Plateau. *Chin. Sci. Bull. (in Chinese)*, *40*(15), 1396–1398. https://doi.org/10.1360/csb1995-40-15-1396

Zhu, L. G. N., and Wu, Z. W. (2023). To what extent can the ozone valley over the Tibetan Plateau influence the East Asian summer precipitation?. *npj Clim. Atmos. Sci.*, *6*(1), 177. https://doi.org/10.1038/s41612-023-00508-x

Ziemke, J. R., Chandra, S., and Bhartia, P. K. (2001). "Cloud slicing": A new technique to derive upper tropospheric ozone from satellite measurements. *J. Geophys. Res.: Atmos.*, *106*(D9), 9853–9867. https://doi.org/10.1029/2000JD900768

Zou, H., Ji, C. P., Zhou L. B., Wang, W., and Jian, Y. X. (2001). ENSO signal in total ozone over Tibet. *Climatic Environ. Res. (in Chinese)*, *6*(3), 267–272. https://doi.org/10.3878/j.issn.1006-9585.2001.03.01

# Supplementary Information for "Impacts of ENSO on wintertime total column ozone over the Tibetan Plateau based on the historical simulations of community Earth system model"

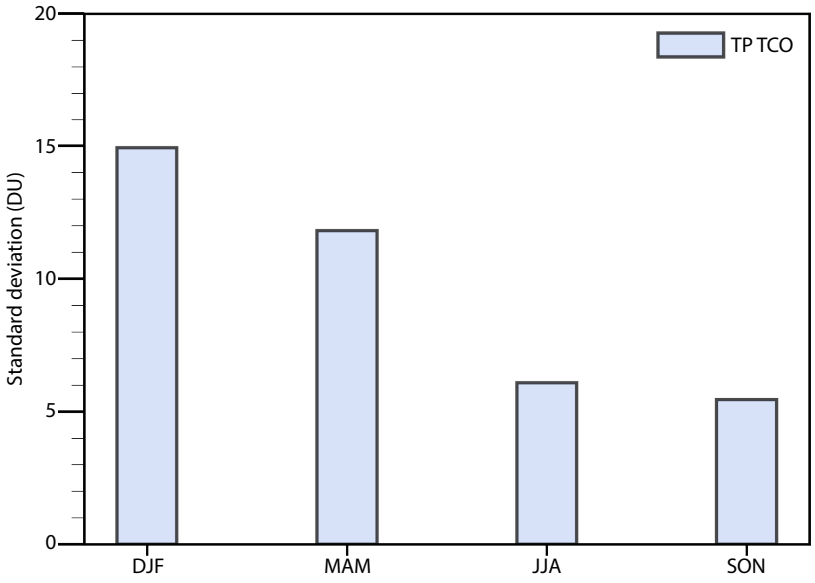


**Figure S1**. Standard deviations (DU) of TP TCO during 4 seasons for C3S dataset.

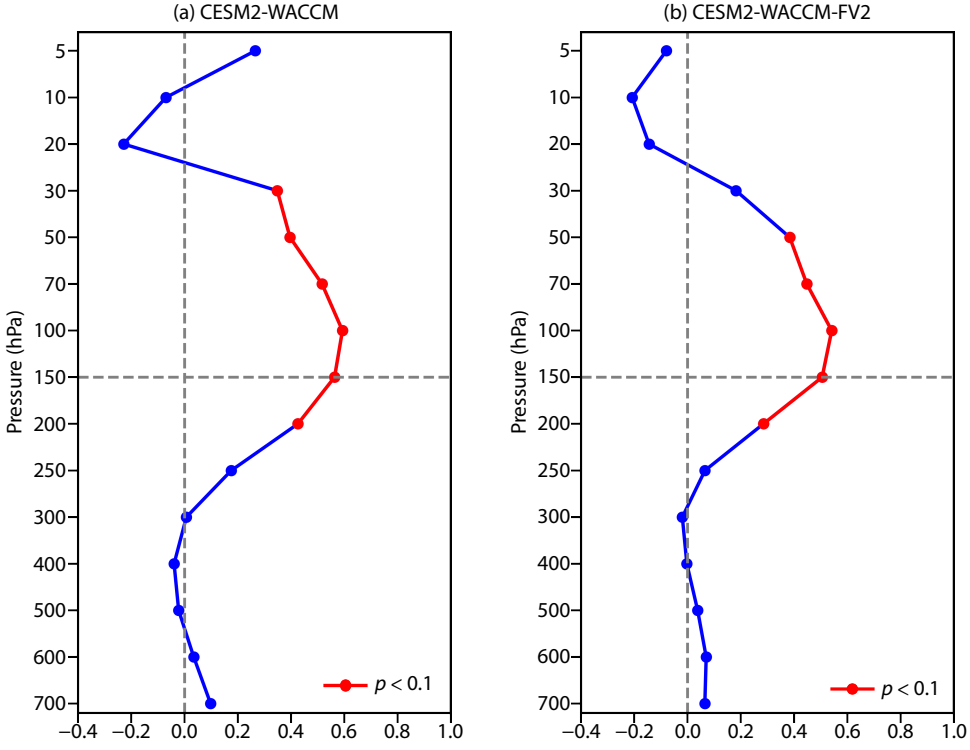


**Figure S2**. The correlation between percentage change (%) of the ozone concentration over the TP and the Niño3.4 index during winter from 1979 to 2014 for the (a) CESM2-WACCM and (b) CESM2-WACCM-FV2 model simulations. The horizontal gray dashed line represents 150 hPa pressure layer, the vertical gray dashed line represents the correlation coefficient zero line, and the red curve represents the correlations exceed the 90% confidence level or the probability value that is less than 0.1 ($p < 0.1$).

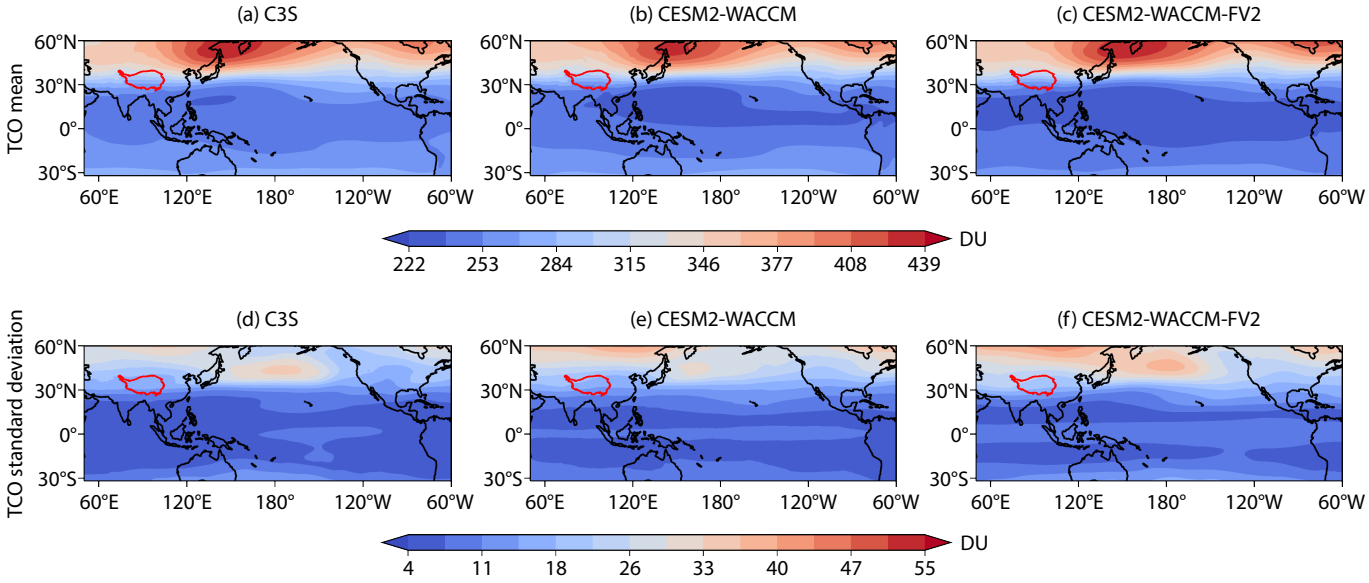


**Figure S3**. (a–c) Climate mean state and (d–f) standard deviation of total column ozone (TCO, Unit: DU) over the East Asia-Pacific during winter (December–January–February; DJF) from 1979 to 2014 for C3S satellite observation, CESM2-WACCM model, and CESM2-WACCM-FV2 model.

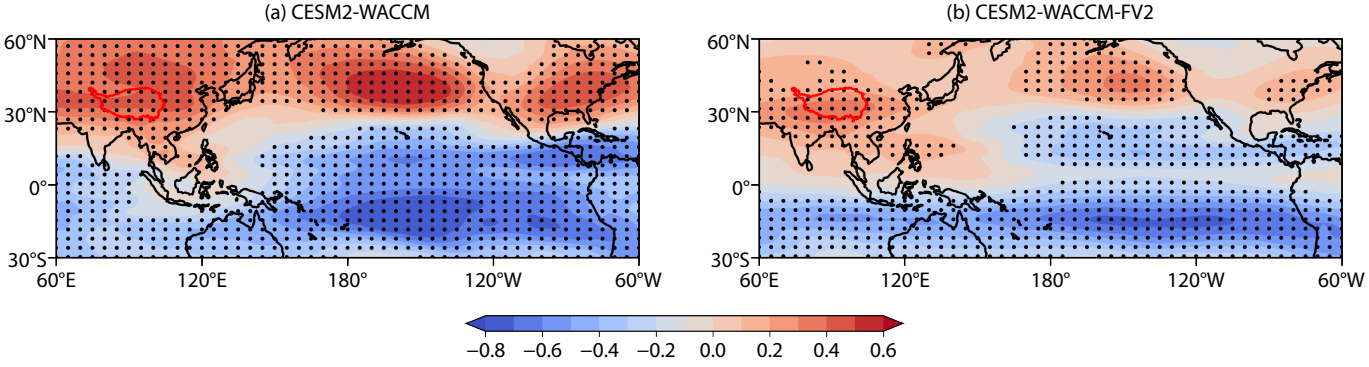


**Figure S4**. The correlation pattern between the TCO anomalies over the East Asia-Pacific and the Niño3.4 index during winter from 1979 to 2014 for the (a) CESM2-WACCM and (b) CESM2-WACCM-FV2 model simulations. Dotted regions indicate statistical significance at the 90% confidence level.

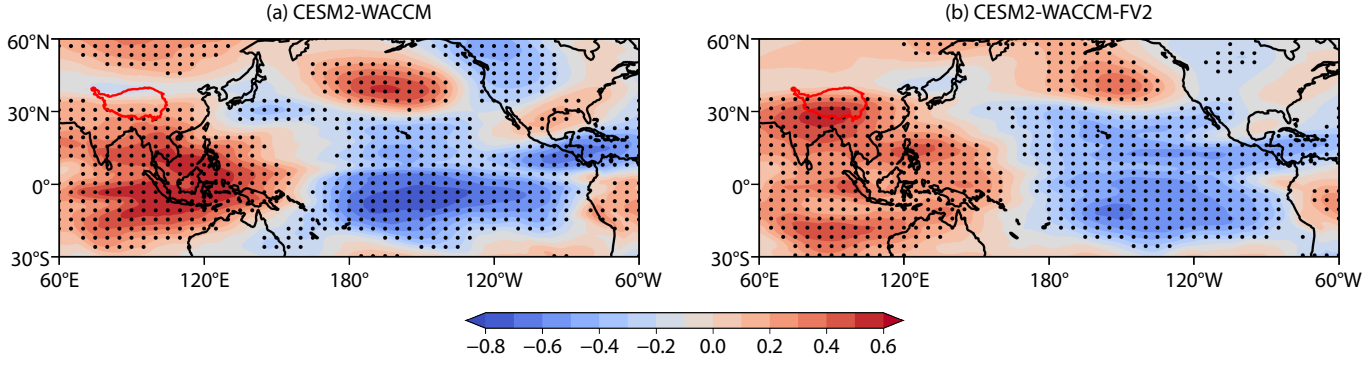


**Figure S5**. The correlation pattern between the zonal TCO anomalies over the East Asia-Pacific and the Niño3.4 index during winter from 1979 to 2014 for the (a) CESM2-WACCM and (b) CESM2-WACCM-FV2 model simulations. Dotted regions indicate statistical significance at the 90% confidence level.

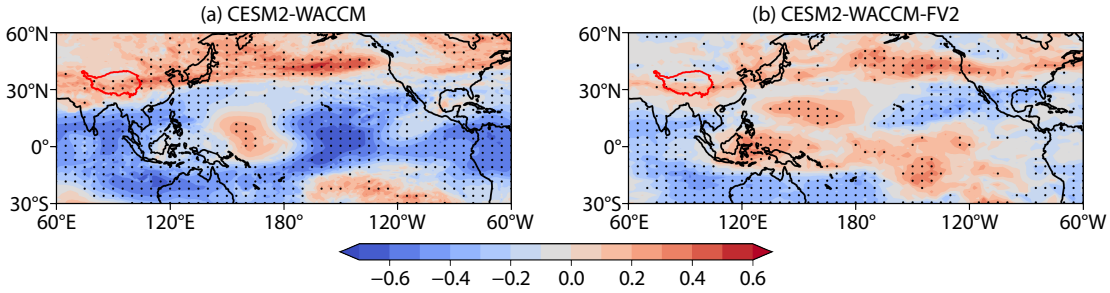


**Figure S6**. The correlation pattern between the tropopause pressure anomalies over the East Asia-Pacific and the Niño3.4 index during winter from 1979 to 2014 for the (a) CESM2-WACCM and (b) CESM2-WACCM-FV2 model simulations. Dotted regions indicate statistical significance at the 90% confidence level.

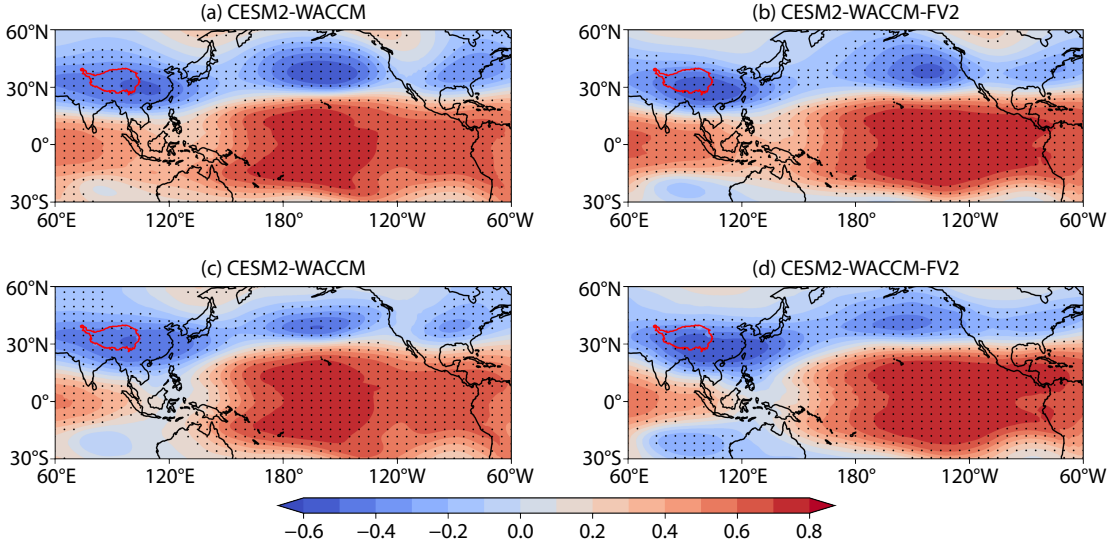


**Figure S7**. The correlation pattern between the wintertime Niño3.4 index and (a–b) 150 hPa geopotential pressure anomalies over the East Asia-Pacific, as well as (c–d) the air temperature associated with the thickness of the East Asia-Pacific from 1979 to 2014 for CESM2-WACCM and CESM2-WACCM-FV2 model simulations. Dotted regions indicate statistical significance at the 90% confidence level.

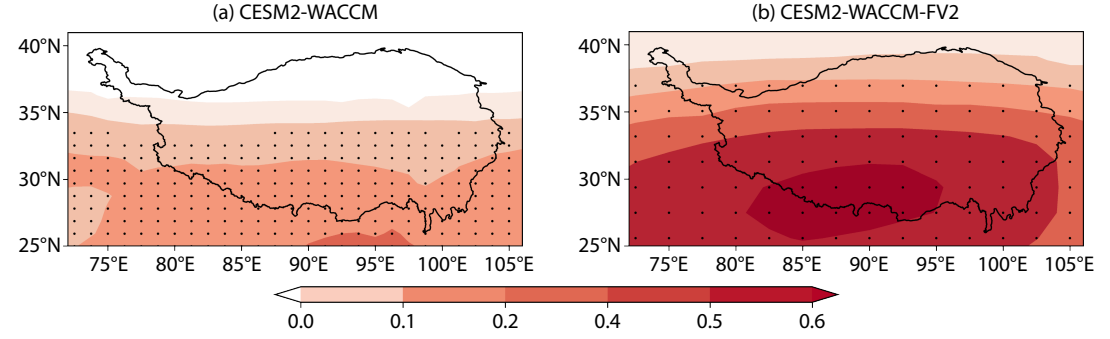


**Figure S8**. The correlation pattern between the zonal TCO anomalies over the TP and the Niño3.4 index during winter from 1979 to 2014 for the (a) CESM2-WACCM and (b) CESM2-WACCM-FV2 model simulations. Dotted regions indicate statistical significance at the 90% confidence level.